

UC Berkeley

UC Berkeley Previously Published Works

Title

Improved Stability and Exciton Diffusion of Self-Assembled 2D Lattices of Inorganic Perovskite Nanocrystals by Atomic Layer Deposition

Permalink

<https://escholarship.org/uc/item/1ks3j1vc>

Journal

Advanced Optical Materials, 8(20)

ISSN

2195-1071

Authors

Lorenzon, Monica
Jurow, Matthew
Hong, Min Ji
[et al.](#)

Publication Date

2020-10-01

DOI

10.1002/adom.202000900

Peer reviewed

Improved Stability and Exciton Diffusion of Self-Assembled 2D Lattices of Inorganic Perovskite Nanocrystals by Atomic Layer Deposition

Monica Lorenzon,* Matthew Jurow, Min Ji Hong, Yi-Hsien Lu, Edward S. Barnard, Miquel Salmeron, Yi Liu, Erika Penzo, Adam M. Schwartzberg, and Alexander Weber-Bargioni*

Colloidal inorganic perovskite nanocrystals (PNCs) are solution-processable optoelectronic materials whose emission can be easily tuned via both size and composition while maintaining high photoluminescence quantum yield. Despite their relative defect tolerance, they suffer from photoinduced damage and degradation under ambient conditions. The lack of long-term stability is addressed by investigating how a ≈ 3 nm transparent ceramic coating applied onto a thin layer of close-packed PNCs via atomic layer deposition (ALD) affects the exciton mobility across the PNCs. Samples coated via both thermal and plasma ALD are compared, as well as an uncoated one. Exciton diffusion measurements yield a record value for all samples, up to $\lambda_D = 480 \pm 24$ nm, one order of magnitude larger than the previously reported values for chalcogenide quantum dots and more than two times larger than what was previously found for the PNCs. Moreover, the ALD-coated samples show stable photoluminescence intensity and energy over 1 year time span. The measurement approach allows for discerning minimal variations in the local luminescence and qualitatively correlating them to the samples' morphology. Hence, it is shown that PNCs coated with an ultrathin ALD film become a very versatile optoelectronic material that can be employed in devices beyond proof of principle.

colloidal synthesis in 2015,^[2] ample work has been published featuring the excellent optoelectronic properties of these solution-processable materials,^[3] from the emission tunability via size, composition,^[2,4] and doping,^[5] to the high quantum yields (QY) despite significant structural disorder.^[6] These advantages make PNCs particularly suitable for a variety of applications such as solid-state lighting,^[7] lasing,^[8] solar cells,^[9] and luminescent solar concentrators (LSCs).^[10] Despite the vast literature devoted to understanding and optimizing their optical properties and some impressive proof of principle devices,^[11] PNCs sensitivity to light, temperature, and environmental exposure has thus far prevented their use in widely functional optoelectronic devices. Moreover, such limited stability prevents a thorough study of exciton transport at the nanoscale, which is pivotal in understanding and optimizing the PNCs optoelectronic properties towards the realization of efficient devices.

1. Introduction

Perovskite nanocrystals (PNCs) have recently become the subject of intense research efforts.^[1,2] After the first report of their


One way to assess their potential for optoelectronics application is by investigating their exciton transport with exciton diffusion measurements. Exciton diffusion mediated by Förster resonance energy transfer (FRET) is responsible for very efficient energy transport in several processes in nature, for instance photosynthesis, but also in artificial systems, such as in quantum dots (QDs) solids.^[12] In the latter case, it is possible for an exciton to hop onto an adjacent QD by FRET mechanism, provided that other conditions for FRET beyond the short distance are met, for instance a significant degree of spectral overlap between the emission spectrum of the excited QD and the absorption spectrum of the ground state QD that is receiving the exciton. Our group has recently demonstrated FRET-mediated transport in a carefully engineered system that allowed to create long-range ordered 2D lattices of close-packed PNCs^[13] and obtain a record transport of 200 nm,^[13] one order of magnitude larger than what previously observed in close-packed arrays of inorganic QDs (30 nm)^[14] and PNCs assemblies (up to 50–70 nm).^[15] Here, we expanded our investigation by reporting for the first time a complete spectrally resolved map of the exciton diffusion spot in a similar

Dr. M. Lorenzon, Dr. M. Jurow, M. J. Hong, Dr. Y.-H. Lu, Dr. E. S. Barnard, Dr. Y. Liu, Dr. E. Penzo, Dr. A. M. Schwartzberg, Dr. A. Weber-Bargioni
The Molecular Foundry

Lawrence Berkeley National Laboratory
Berkeley, CA 94720, USA

E-mail: monicalorenzon@lbl.gov; afweber-bargioni@lbl.gov

Dr. M. Lorenzon, Dr. M. Jurow, Dr. Y.-H. Lu, Dr. M. Salmeron, Dr. Y. Liu
Materials Sciences Division
Lawrence Berkeley National Laboratory
Berkeley, CA 94720, USA

 The ORCID identification number(s) for the author(s) of this article can be found under <https://doi.org/10.1002/adom.202000900>.

© 2020 The Authors. Published by WILEY-VCH Verlag GmbH & Co. KGaA, Weinheim. This is an open access article under the terms of the Creative Commons Attribution License, which permits use, distribution and reproduction in any medium, provided the original work is properly cited.

DOI: 10.1002/adom.202000900

self-assembled close-packed monolayer of PNCs. Importantly, the spectral resolution gives complementary information to the time-resolved map, shining light on the spatially dependent spectral change that could be either due to thermalization onto larger PNCs (with smaller energy gaps) or due to defects.

The ability of an exciton to travel for long distances without perturbations is of great importance in optoelectronic applications. In order to promote this, one needs to implement strategies to maintain the optical stability over time. Therefore, in this manuscript, we expand the work we did in the previous work^[13] by comparing samples with two differently processed protective coatings. Recently, several passivation strategies have been explored in order to overcome the stability issues that hinder the actual employment of PNCs in optoelectronic devices,^[16] most commonly, crosslinking of the surface ligands^[17] or the application of polymeric coatings.^[18] Atomic layer deposition (ALD) is another promising passivation technique that eschews complex synthetic steps and provides durable ceramic barriers for protecting the PNCs against exposure to humid air, oxygen, and other environmental factors that can affect their optical and structural shelf life, with thicknesses controllable to a sub-angstrom level.^[19] Recently, protective dielectric films with overall thickness ≈ 50 nm grown by ALD have been shown to significantly improve the long-term stability of PNC thin films up to 45 days.^[16b] In our previous work,^[13] we relied on plasma ALD to deposit an ultrathin (3 nm) alumina layer. Here, we expanded such study by preparing and comparing two monolayer films of close-packed cesium lead bromide (CsPbBr₃) PNCs from the same colloidal suspension. We coated them with a 3 nm thick layer of alumina, deposited by either thermal^[19a,20] or plasma^[21] assisted ALD, in order to address some critical issues: 1) achieving a long-term stability (up to 1 year) of both optical and structural properties; and 2) ensuring that these properties are not affected by the deposition process.

We, therefore, performed a suite of optical characterizations on the two samples, measuring their photoluminescence (PL) spectra and their lifetimes over a time span of 1 year, as well as performing a detailed investigation of the exciton diffusion in our samples. The high resolution of our setup allowed us to discern slight, but very relevant, differences between them, while also recording an exceptional diffusion length of over 400 nm. We found that both the plasma and the thermal processes provide an effective coating that preserved the PNC optical properties. In each case, after an initial depreciation over 4 months, both samples reached an optically stable state, which remained unchanged for over 1 year. Our work highlighted the feasibility of ALD surface passivation, demonstrating that an ultrathin layer of ALD alumina (≈ 3 nm) is sufficient to ensure stable optical properties after 1 year. Moreover, the exceptional exciton diffusion lengths recorded for our ALD-coated PNCs films constitutes a remarkable result towards their actual integration into photonic and optoelectronic devices.

2. Results and Discussion

2.1. Sample Architecture and Optical Characterization

In order to examine the effect of ALD growth on the PNC surface, it is necessary to remove all other layers and work only on close-packed monolayer films. By spin coating from

toluene solutions of PNCs, monolayers are deposited on $-\text{CH}_2$ -terminated polymer functionalized surfaces.^[11d,13] A fundamental characterization of the as-synthesized sample is reported in the Supporting Information (see Figure S1a–c, Supporting Information, for optical absorption and PL intensity, X-ray diffraction, and transmission electron microscopy, respectively). Spin-coating parameters are optimized to achieve a close-packed monolayer (see Experimental Section for details).^[13] The samples are then ready for ALD (Figure 1a). We used two distinct ALD processes, namely, a thermal process and a plasma process, to compare the effect of the different conditions for depositing the protective layer on the perovskite monolayer. We leave left one sample uncoated for comparison. In Figure 1b,c, we report the optical performance of the three samples (thermal, plasma, and uncoated) after preparation. The normalized PL intensity shows a peak centered at 518 nm for the samples with an ALD coating, with a full width at half maximum (FWHM) of 16 and 20 nm for the thermal and plasma samples, respectively. The main peak of the uncoated sample is slightly redshifted, centered at 523 nm (FWHM = 18 nm), likely due to a prompt and irreversible degradation of the PNCs upon exposure to light and/or air (Figure 1b). In order to make sure that the whole deposition process was repeatable, we have prepared and optically characterized three samples for each kind. In Figure S2, Supporting Information, we report the time-resolved PL of all samples for comparison, which show the similarity of the decay traces between each kind of sample.

In addition, the uncoated sample shows a broad, low energy band, usually ascribed to emission from excitons or carriers trapped at the surface in similar systems.^[22] The low energy band is absent in both of the ALD coated samples, consistent with our assumption of fewer surface traps. In order to provide a more quantitative comparison between the optical performances, we measured the radiative lifetime decay traces of each sample (Figure 1c). The thermal ALD sample featured a double exponential decay whose slow component (accounting for $>70\%$ of the signal) exhibited a 5 ns lifetime. A very similar lifetime (4.95 ns, $>70\%$ of the signal) is observed for the plasma deposited sample. The fast component accounting for the remaining part of the signal ($<30\%$ in both cases) was slightly different, with a 1.7 ns lifetime for the thermal sample and a shorter lifetime of 1.4 ns for the plasma sample. This difference is likely due to the introduction of nonradiative recombination channels during the coating or differences in coating efficacy. Both the fast and slow components are reported for comparison in Figure 1d for the thermal, plasma and uncoated sample. The latter, as expected, exhibits a significant quenching of its PL emission compared to the coated samples, in terms of both lifetimes and intensity (Figure 1e). The uncoated sample exhibits a double exponential decay with a fast component of 0.9 ns, accounting for 30% of the signal, and a slow component of 4.0 ns, for the remaining 70% of the decay. The PL lifetime and corresponding τ_{fast} and τ_{slow} are reported in Figure S3a,b, Supporting Information.

2.2. Evolution of the Optical Properties Over Time

To investigate the efficacy of the different passivation methods over time, pivotal to assess the viability of our approach for potential applications, we measured the time-resolved PL

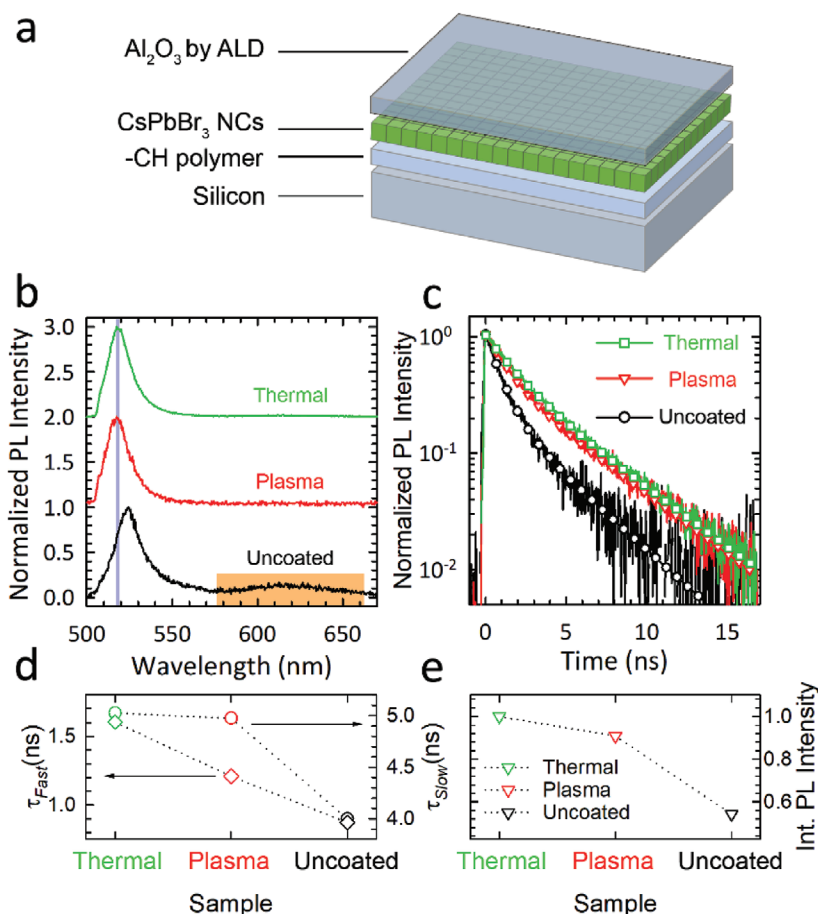


Figure 1. a) Schematic of the sample architecture. Samples consist of a silicon substrate coated with a 10 nm thick $-CH$ -terminated polymer. $CsPbBr_3$ NCs (10 nm edge lengths) are deposited onto this layer and coated with a 3 nm layer of Al_2O_3 deposited via ALD. b) PL spectra for a set of samples of $CsPbBr_3$ perovskite NCs deposited onto a polymer-coated silicon substrate. The thermal (green line) and plasma (red line) samples are coated with a 3 nm thick layer of Al_2O_3 . An uncoated sample (black line) is measured for comparison. The PL spectra are vertically shifted for clarity. A gray shade is used to highlight the difference in the peak position between the ALD-coated and -uncoated samples. The orange shade indicates the defect-related broad band. c) Normalized time-resolved PL intensities of the same samples reported in (a). The same color code as in (a) applies. The respective double exponential fits are reported onto each decay curve as white dots. d) Fast (left axis, diamonds) and slow (right axis, circles) components of the double exponential decays and relative fits reported in (c). The same color code as in (b) and (c) applies. e) Integrated PL intensity of the three samples as in (b), (c) and (d), normalized to the intensity of the thermal sample. All measurements are performed at room temperature under 465 nm pulsed excitation.

intensity of our samples (Figure 2a,b) at the time of preparation, after 1 month of exposure to ambient air (with a relative humidity of $40\% \pm 10\%$), after three additional months (4 months in total), and eventually 1 year in total. The two samples exhibited a similar behavior, with a degradation in the optical properties that proceeded steadily over a 4 month period and then saturated and remained constant. Importantly, this plateauing of the optical degradation suggests that the thin ALD coating effectively acts as a barrier that prevents humid air and oxygen from permeating further after a few months, which is very important for the actual employment of PNCs monolayers into any optoelectronic applications. The thermal sample maintained a better decay trace overall, but both were significantly better than the uncoated sample, whose lifetime decreases soon after the PNCs deposition process takes place.

In order to better investigate the impact of the coating mechanism at critical length scale, we recorded atomic force microscopy (AFM) and scanning electron microscopy (SEM) images of

both films after the stabilization of their optical properties (that is, ≈ 4 months) and observed very different morphologies. The AFM image of the thermal sample (Figure 2c) showed a significant number of large cube-like structures (up to 80 nm on edge), which are absent from the plasma sample AFM (Figure 2d).

These results were confirmed by SEM (Figure 2e,f). While the thermal film coverage appeared to be slightly more uniform, featuring a lower root mean square value measured by AFM (3.0 ± 0.4 and 3.8 ± 0.2 nm for the thermal and plasma samples, respectively), it also displayed significant changes in the film morphology, resulting in the observed uniform distribution of large cubic aggregates. Such sintering of the PNCs into larger structures likely stemmed from a combination of water, temperature, and the ultrathin layer of PNCs. The thin film is more sensitive to structural annealing effects than thicker multilayer films. Nonetheless, access of water and oxygen molecules to the PNCs is limited enough to allow a partial preservation of the optical properties over time.

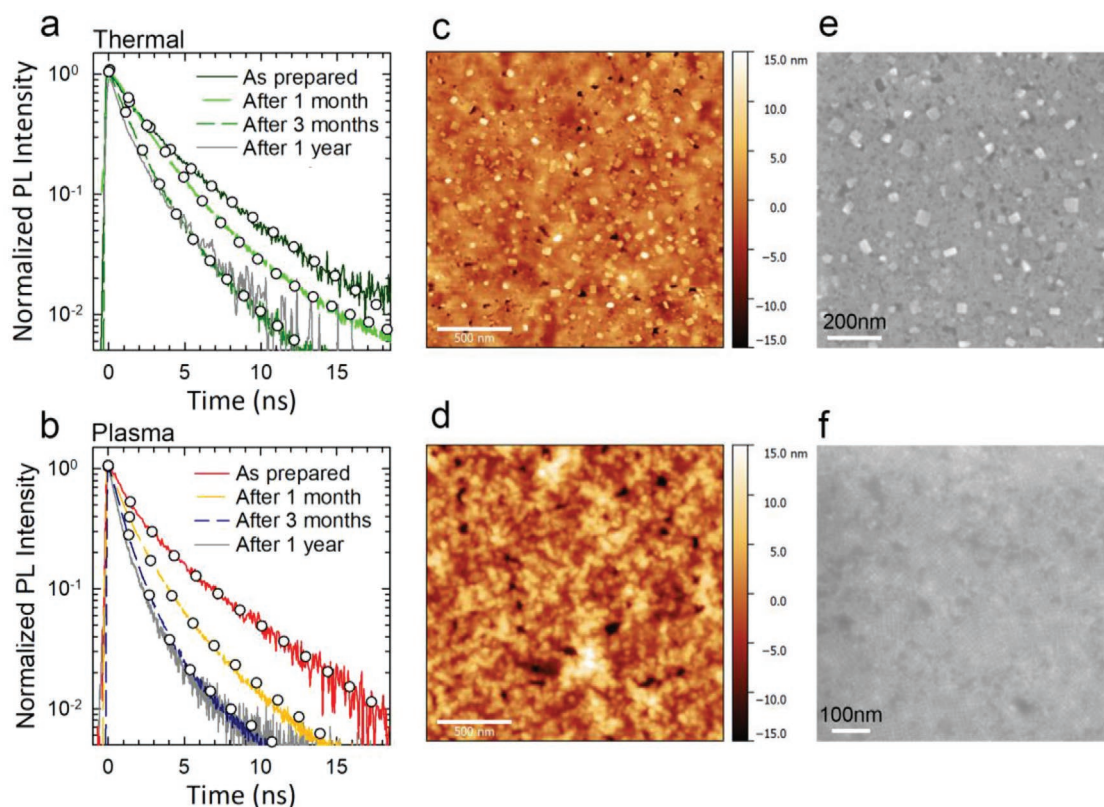


Figure 2. Normalized time-resolved PL intensities for a film of NCs coated by a) thermal and b) plasma ALD deposition of aluminum oxide, measured immediately after the sample preparation, after 1 month, after 3 months (colored lines), and after 1 year (solid gray line). All decay traces are fitted with double-exponential curves and all the fits are reported with white dots. AFM images of a portion of the c) thermal and d) plasma samples after 4 months (i.e., after the optical stabilization is reached), yielding root mean square values of 3.0 ± 0.4 and 3.8 ± 0.2 nm for the thermal and plasma samples, respectively. The scale bar is 500 nm. SEM micrographs of the e) thermal and f) plasma samples. Scale bar is 100 nm. Both the AFM and SEM images were collected after 4 months from the sample deposition. All measurements are performed at room temperature under 465 nm pulsed excitation.

In order to test if increasing the water content during the thermal process negatively affects the optical properties, we coated two PNC monolayers with thermal ALD at different water pressures (80 and 150 mTorr). The PL spectra (Figure 3a) and decay traces (Figure 3b) showed no difference between the two pressures, without any defect-related band, unlike the uncoated sample that was made for comparison, suggesting that the increased pressure does not generate additional defects. As for the decay traces, similarly to what was already observed in the initial thermal sample, there was a degradation over time that eventually saturates after a 4 month time span, but no difference between the two pressures was observed. SEM images on both samples (Figure 3c,d) confirmed the formation of large structures all over the samples, with a similar concentration, suggesting that the increasing pressure does not introduce more defects or promote significantly more sintering of the PNCs.

2.3. Investigating the Steady-State Exciton Diffusion

Despite the significant morphological changes occurring to the thermal sample upon deposition of the alumina coating, there was no sign of a significant change in the PL spectra

of the overall sample. This is not surprising, since this material system lies in the weak confinement regime, with a Bohr diameter of 7 nm for CsPbBr₃, smaller than the 10 nm-side cubes. As a result, the emission from larger cubes occurs from the same excitons without any noticeable red shift due to the larger cubes. On the other hand, it can reasonably be inferred that the presence of large cubes affects the motion of excitons through the sample. Exciton diffusion is particularly important for light-harvesting applications. In order to verify this assumption and to further explore the actual potential of our system for optoelectronic applications, we performed a set of exciton diffusion measurements on the samples and investigated how the different protective coatings, thermal versus plasma, affect the diffusion process. In our previous work,^[13] we thoroughly discussed the exciton diffusion dynamics on a similar close-packed monolayer of perovskite nanocubes and reported a record diffusion length of 200 nm. Here, we built on this work to study the diffusion process by comparing the plasma, thermal and uncoated sample via steady-state and spectrally resolved diffusion measurements. The close-packed distribution of our emitters is pivotal to achieve such results, since the distance between the PNCs enables an efficient FRET process while the monolayer provides a strong constraint for confining the excitons motion in a 2D plane. As a result, it

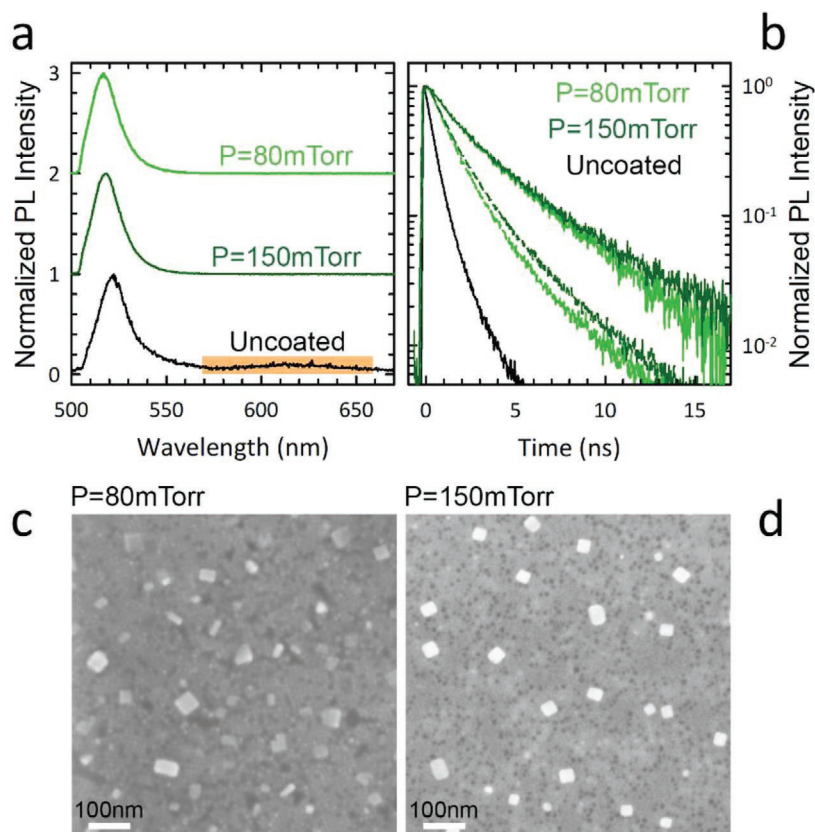


Figure 3. a) PL spectra for a set of samples of CsPbBr₃ perovskite NCs deposited onto a polymer-coated silicon substrate, coated with ALD deposited aluminum oxide by thermal process at two different water pressures, namely, $P = 80$ mTorr (light green) and $P = 150$ mTorr (dark green). An uncoated sample (solid black line) is measured for comparison. The PL spectra are vertically shifted for clarity. The orange shade indicates the defect-related broad band. b) Normalized time-resolved PL intensities for a film of NCs coated by thermal ALD deposition with different water pressure, namely, $P = 80$ mTorr and $P = 150$ mTorr (light and dark green, respectively), as long as with an uncoated sample used for comparison (solid black line). The thermally coated samples are reported after preparation (solid green lines) and after three additional months (dashed green lines). All optical measurements were performed at room temperature, under 465 nm pulsed excitation. SEM micrographs of the thermally coated samples at c) $P = 80$ mTorr and d) $P = 150$ mTorr after 4 months from the sample preparation. Scale bar is 100 nm.

was possible to directly visualize the exciton diffusion in two dimensions and to study and compare results between different samples.

We started by perpendicularly exciting the samples with a diffraction limited laser spot (see Figure 4a, top panel). The nominal FWHM for a 465 nm excitation wavelength with an air objective with $NA = 0.95$ would be 245 nm. We found an average value of 297 nm due to the convolution of the laser beam with the point spread function (PSF) of our optical system, which we use later to calculate the diffusion length. By focusing the laser beam onto our sample, a local population of excited states is generated, with an initial spatial distribution that mirrors the laser beam profile. If an exciton generated onto a PNC is able to hop onto adjacent, non-excited PNCs, then the initially excited population undergoes a radial diffusion process that, similarly to any diffusion described by the Fick's laws, stems from a concentration gradient (in this case, concentration of excitons) and results in a broadening of the initial Gaussian profile over time and space. Hence, by filtering out the excitation, we collected the image of the PL that is spatially broader than the excitation spot, with an increase in the spot

size that depends on the ability of the excitons to hop onto a neighbor before recombining.

The collected PL was sent to a high-definition CCD camera, where we recorded the spatially resolved diffusion profile. If the sample exhibits any diffusion, the collected spot will be broader than the excitation spot, as illustrated by the 3D Gaussian profiles in Figure 4a for the incoming laser beam (top panel) and the PL (bottom panel). An example of raw diffusion images collected with the camera is reported in Figure 4b, showing the excitation spot (first image) and the PL map for the three samples, uncoated, thermal, and plasma respectively, providing a first qualitative overview of the results. All three samples show a significant amount of diffusion compared to the excitation spot, but the thermal and plasma samples exhibit a stronger PL intensity and a slightly broader PL spot. Importantly, all images show a complete degree of symmetry of the radial diffusion, which suggests that there are no additional effects causing any anisotropy in the direction of the excitons motion and therefore in the diffusion profile.

In order to better analyze the image, we extracted one line of the raw PL intensity image (passing through the center) and plotted it as a function of space. Figure 4c reports the average

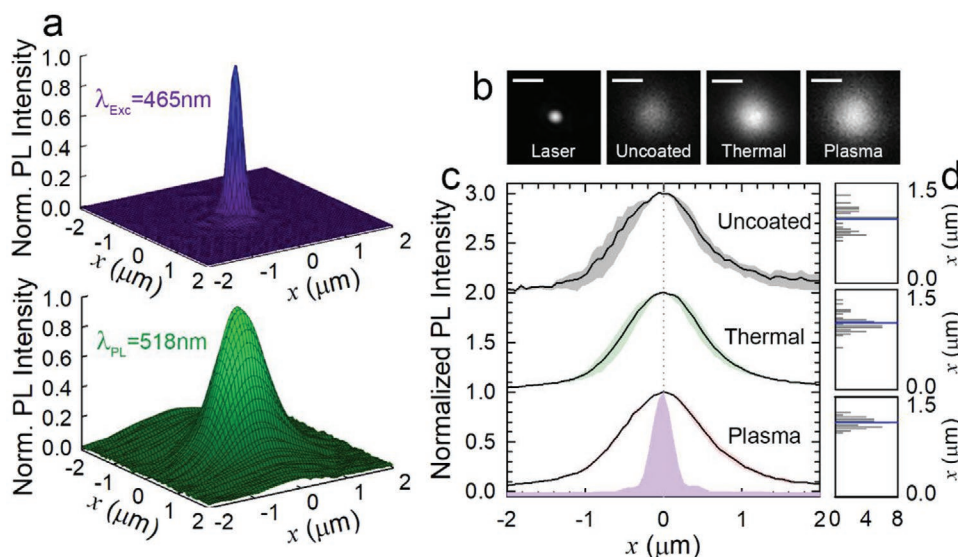


Figure 4. a) Representative 3D mesh plots of a 465 nm laser spot (top panel) and relative larger PL at ≈ 518 nm, collected by filtering out the laser light, due to exciton diffusion in the thermal sample. b) Raw images recorded with a square CCD for the laser spot at 465 nm (first image) and for the PL, collected by filtering out the laser light, of the uncoated, thermal, and plasma samples. The original images are cropped around the diffusion spot for clarity. Scale bar is 1 μm in all images. c) Diffusion profiles for the uncoated, thermal, and plasma samples (black solid lines) averaged over more than 50 measurements for each sample. The colored shade (gray, green, and red for uncoated, thermal, and plasma, respectively) represents the average trend \pm the standard deviation, which is found to be 19%, 12%, and 5% for the uncoated, thermal, and plasma samples, respectively. d) Statistics of the average values measured for the three samples (uncoated, thermal, and plasma as top, center, and bottom panels). The average is reported with a solid blue line and is 0.9 ± 0.2 , 1.07 ± 0.13 , and 1.21 ± 0.06 μm for the uncoated, thermal, and plasma, respectively.

PL profile for each sample (uncoated, thermal, and plasma, respectively, starting from the top) calculated from more than 50 images collected for each sample. The laser profile is displayed as a purple shade for comparison. A first glance at the Gaussian profiles immediately allows one to appreciate a large FWHM, around 1 μm , for all samples, compared to the laser profile. Deconvolving the Gaussian profile^[13] shows exciton diffusion lengths of over 400 nm. However, there is a significant difference in the standard deviation for the three samples, which results in a percentage error with respect to the average value of 19%, 12%, and 5% for the uncoated, thermal, and plasma samples, respectively. Such difference can also be appreciated in the histograms of the FWHM counts reported in Figure 4d, which shows a broader distribution compared to the average value (reported as a solid blue line for all samples) with respect to the uncoated sample. Both data hint to an overall better uniformity of the coated samples, resulting in more consistent measurements of the diffusion profiles. Moreover, both the profiles and the average values on the statistic plots (all reported with the same y scale) suggest that a larger FWHM value is obtained for the coated samples and more specifically for the plasma, leading to an exceptional value of 1.21 ± 0.07 μm of FWHM. By using the steady-state formula for calculating the diffusion length, we obtain $\lambda_D = 480 \pm 24$, 436 ± 52 , and 421 ± 80 nm for the plasma, thermal, and uncoated samples, respectively. It is worth to notice that this exceptional result is in part due to the ALD coating, which helps preserving the optical properties over time, and in part to the longer lifetime compared to our previous results. Having an average lifetime more than twice as long results in more hops across PNCs, and therefore longer travel distances.

2.4. Exploring the Spectrally Resolved Exciton Diffusion

After obtaining a first evaluation of the quality of the film via a steady-state measurement of the exciton diffusion, we performed a spectrally resolved scan of the diffusion profiles. In this case, we relied on a custom-built feature of our setup that allows one to excite the sample with a diffraction limited laser spot and collect the magnified PL emission (100 \times) by a single-mode fiber. Such fiber was mounted on a translation stage that systematically scans the fiber aperture in the focal plane of the microscope and sends the collected light to a spectrometer in order to provide spectral resolution and collect a PL spectrum at each fiber position. By reporting the PL spectra collected for each step over the diffusion profile, we obtained the contour plots reported in Figure 5a for the uncoated, thermal, and plasma samples, respectively, starting from the top. Each measurement was centered at a 0 μm distance, corresponding to the position of the fiber that is coaligned with the center of the excitation/diffusion spot. Distances greater than zero represent the distance between the center of the PL spot and the center of the image of the fiber aperture on the sample plane.

A few differences were immediately evident, such as, for example, the red shifted emission of the uncoated sample, corresponding to the PL recorded for the whole sample. Moreover, the maxima of each PL spectra (highlighted with a solid white line) were not a straight line for all samples, but rather display some curvature. In order to analyze these measurements in greater detail, we extracted and plotted data from the contour plots.

The intensity profile of the scanned spot over space is very similar to the profile extracted from a spatially resolved image,

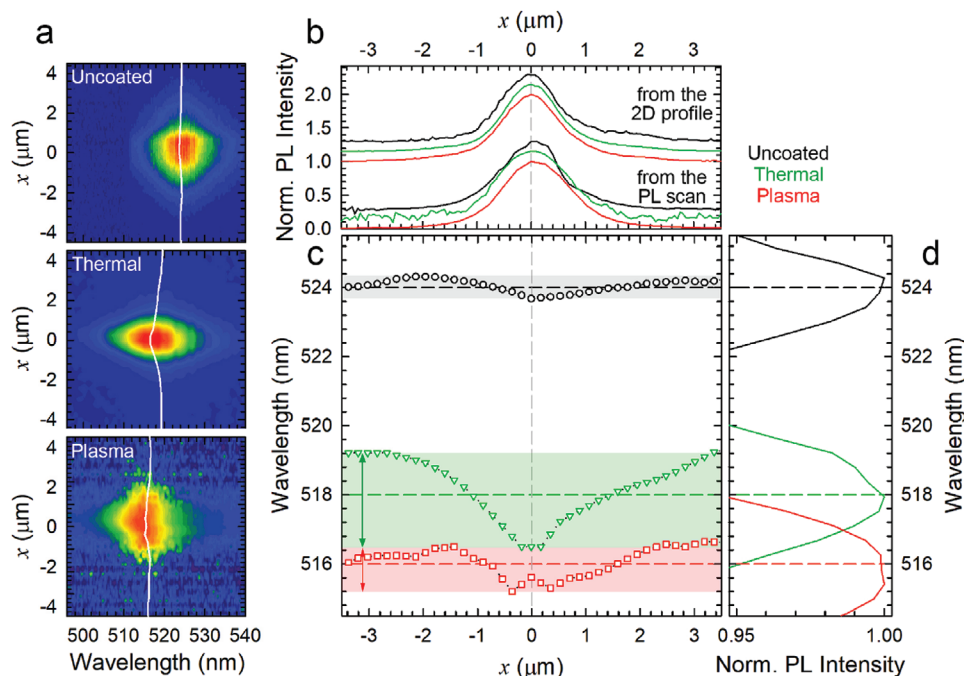


Figure 5. a) Contour plot of the spectrally resolved diffusion for the uncoated, thermal, and plasma sample (top, center, and bottom panels, respectively), collected by scanning a 5 m fiber with a translational stage and sending the PL to a spectrometer. The 0 μm distance corresponds to the position of the fiber that is coaligned with the center of the PL diffusion spot. The white line onto each contour plot connects the maxima of each PL spectra. b) PL intensity profile obtained by steady-state exciton diffusion (top black, green, and red solid lines for the uncoated, thermal, and plasma samples, respectively) and by integrating the PL spectra recorded at each fiber position (bottom lines, same color code). c) Wavelengths corresponding to the PL maxima of the spectra collected at each fiber position, as a function of the position. The uncoated, thermal, and plasma samples are reported as black circles, green triangles, and red squares, respectively. The wavelength shift is highlighted by colored shades. d) PL spectra of the overall diffusion spot for each sample, highlighting the correspondence of the wavelength maxima in (c) with the measurements across the whole diffusion spot. All measurements are performed at room temperature, under 465 nm pulsed excitation.

as those shown in Figure 4. In Figure 5b, we reported the Gaussian-like profiles as extracted from the images in Figure 4b (top three profiles in Figure 5b) and the intensity profiles extracted as vertical slices from Figure 5a (bottom three profiles, for uncoated, thermal, and plasma starting from the top, respectively). The two set of profiles are very similar, with the only difference that the set extracted from the PL scan appears noisier due to little light being collected at each step. Interestingly, as anticipated, the most significant difference in the PL spectra scans lies in the positioning of the PL maxima over the spatial scan. Specifically, a red shift is observed while transitioning from the center of the excitation spot towards the outer edges, as highlighted by the solid white lines in Figure 5a. In order to better quantify the extent of such red shift for each sample, we plotted the PL maxima as a function of the space for the uncoated, thermal and plasma samples (Figure 5c). The PL maxima of different samples are centered at slightly different wavelengths (namely, 524 nm for the uncoated sample, 518 nm for the thermal, and 516 nm for the plasma), consistently with the PL obtained across the films as shown in Figure 1 and reported here in Figure 5d as a direct comparison.

Then, we observed that the extent of the shift is different for the three samples, as highlighted from colored shades under the trends. Whereas the uncoated sample and the plasma sample exhibit limited redshifts (≈ 0.8 and 1.2 nm, respectively), the redshift is more pronounced in the thermal sample, ≈ 2.8 nm. The

presence of the redshift can be ascribed to a thermalization of the resonant energy transfer onto larger QDs with smaller energy gaps, which lowers the chances of back energy transfer onto a smaller adjacent PNC, and therefore lead to emission from a redshifted dot. The large cubes on the thermal sample likely represent a hindering factor that traps excitons, which are not capable of hopping onto an adjacent PNC.

Moreover, we cannot exclude that the redshift is further enhanced by the presence of surface defects, which would likely be formed during the ALD step due to the presence of water molecules, and that could lead to exciton self-trapping and therefore redshifted emission.

Overall, these measurements confirmed the better quality of the plasma sample, whose diffusion profile is more uniform across the sample and likely less affected by the ALD process which, despite the presence of a plasma, does not introduce any morphological change to the PNC monolayer, thus representing a robust method for the deposition of an ultrathin transparent coating that effectively protects this material system for a significant amount of time.

3. Conclusions

In this work, we simultaneously tackled the PNCs stability issue under ambient conditions while enhancing significantly

the exciton transport through the sample by employing ultrathin aluminum oxide layers. We compare optical and diffusion properties of close-packed, self-assembled thin films of cesium-lead-bromide PNCs, coated with a ≈ 3 nm thick aluminum oxide layer, deposited either by thermal or plasma ALD. In both cases, the transparent Al_2O_3 layer greatly increased the preservation of the PNCs optical properties, as demonstrated by comparison to an uncoated sample. Despite an initial degradation of the time traces over time, both coated samples reached a stable PL after 4 months, which remained unchanged for over 1 year. Considering that perovskite materials easily undergo irreversible degradation due to air and humidity, and that our samples were stored in air at room temperature, this result demonstrated the applicability of this system for optoelectronic devices. On the other hand, the two deposition processes yielded a very different effect on the morphology of the PNC film, with the thermal sample displaying a significant amount of large (tens of nanometers) sintered cubes across the whole sample, which were not present in the plasma sample. This was likely due to a combined effect of water, heat, and a thin monolayer of PNCs during the thermal deposition process, which promoted the sintering of PNCs into larger structures. Conversely, despite the presence of a plasma that may damage the organic ligands of the PNCs and therefore lead to a less uniform coating layer, we did not observe morphological changes in the plasma sample. These changes in the morphology directly affect the motion of excitons across the 2D lattice of self-assembled PNCs, as we showed by performing exciton diffusion measurements on both the coated and uncoated samples. The plasma sample yielded the best results, providing the larger diffusion length, with a record value of $\lambda_D = 480 \pm 24$ nm, which is one order of magnitude larger than previously reported values for traditional chalcogenide QDs^[14] and more than two times larger than what was previously found by our group.^[13] On the other hand, while still obtaining good results in terms of diffusion length, the thermal sample showed a significant redshift (up to ≈ 3 nm) of the PL maxima while looking at the PL spectrum from the center of the excitation spot toward the tails. Such effect is likely due to the thermalization of an exciton onto larger dots or sintered large cubes, from where it cannot be transferred back onto a smaller PNC; surface defects arising during the thermal process may also contribute to the redshift by causing exciton self-trapping onto surface states.

In conclusion, our investigation demonstrated that the addition of an ultrathin transparent, protective layer provides significant benefits to the PNCs monolayer preservation and shelf-life, which is of paramount importance for employing PNCs as optically active materials in actual optoelectronic devices.

4. Experimental Section

Synthesis of CsPbBr_3 PNCs: CsPbBr_3 PNCs were synthesized by a procedure adapted from the original report.^[2] All chemicals were purchased from Sigma-Aldrich and used as received without further purification. Cs_2CO_3 (1.2 mmol) was added to 10 mL 1-octadecene and stirred at 120 °C under vacuum for 1 h. Oleic acid (2 mmol) was injected under nitrogen atmosphere and resulting mixture was stirred at 120 °C for 2 h until fully dissolved. In a separate container, PbBr_2 (0.19 mmol) was added to 5 mL 1-octadecene and stirred at 120 °C under vacuum for 1 h. Oleic acid (1.6 mmol) and oleylamine (1.5 mmol) were injected

under nitrogen atmosphere. The resulting mixture was stirred at 120 °C for 2 h until fully dissolved, then was heated to 165 °C. A total of 0.4 mL of hot Cs_2CO_3 solution was added to this preheated solution under nitrogen atmosphere with vigorous stirring. Reaction was stirred for 5 s and cooled rapidly in an ice bath until the reaction mixture solidified.

After freezing, the reaction mixture was warmed to room temperature and transferred into centrifuge tubes. The mixture was centrifuged at 8500 rpm for 10 min. The supernatant was discarded, and the pellet was redispersed in anhydrous hexane (6 mL). An equal volume of *tert*-butanol was added to precipitate the nanocrystals, and the mixture was centrifuged at 12 000 rpm for 15 min. The supernatant was discarded, and the pellet was dispersed in toluene. These solutions were then centrifuged for 5 min at 700 rpm, and the pellet was discarded to remove large aggregates. The supernatant was transferred to a glove box for film deposition.

Sample Preparation: PNC close-packed thin films were prepared by spin coating (1500 rpm, 45 s) from a colloidal suspension of CsPbBr_3 PNCs in toluene (3 g L^{-1}) onto Si wafers coated with 10 nm of a $-\text{CH}$ -terminated polymer. The hydrocarbon polymer was deposited by polymerizing methane in a plasma chamber (40 mTorr, RF power 100 W, 10 °C, Oxford Instruments). Aluminum oxide (3 nm) was deposited via either thermal- or plasma-assisted ALD at 40 °C (FLEXAL, Oxford Instruments). Deposition details are as follows: trimethylaluminum at 30 °C, dosed by vapor draw. Thermal process at 40 °C: TMA dose—25 ms, 80 mTorr; TMA purge—5 s; water dose—30 ms, 80 mTorr; water purge—7 s. Plasma process at 40 °C: TMA dose—25 ms, 80 mTorr; TMA purge—5 s; plasma dose—1 s, 40 mTorr; water purge—4 s.

Deposition rates were characterized by ellipsometry (Horiba UVVISSEL spectroscopic ellipsometer) and were found to be 0.074 nm per cycle for the thermal process and 0.17 nm per cycle for the plasma process. In order to deposit the target 3 nm thickness, the thermal process was run for 40 cycles while the plasma process was run for 17 cycles. All films were characterized by SEM (Zeiss).

Time-Resolved and Spectrally Resolved PL Spectroscopy: A pulsed laser source (center wavelength 465 nm with a 2.5 nm bandwidth; 5 ps pulse duration; 40 MHz repetition rate; $0.1 \mu\text{J cm}^{-2}$ fluence) was collimated and focused by a 100×0.95 NA objective lens. The back aperture of the objective was overfilled to ensure diffraction-limited performance. Emission from the sample was collected by the same objective and directed onto a 300 μm diameter fiber (Thorlabs) coupled to an Ocean Optics Flame spectrometer to obtain the PL spectra. The time-resolved measurements were performed by sending the signal to a single-photon counting avalanche photodiode (MPD PDM-series) connected to a time-correlated single-photon counting unit (PicoHarp 300). The temporal resolution was ≈ 50 ps, as determined by the FWHM of the instrument response function. For the exciton diffusion scan, the emission from the sample was collected by the same objective and imaged onto a single-mode fiber (PI-405P-FC-2, Thorlabs) mounted onto a translation stage (attocube ECS series) that scanned the emission focal plane. The stage was moved in 5 μm steps corresponding to 50 nm at the sample. A 490 nm long-pass dichroic filter (Semrock) and two 496 nm long-pass edge filters (Semrock) were used to remove the excitation laser beam from the PL signal. The laser beam was imaged through the 490 nm long-pass dichroic filter (Semrock) and a 498 nm short-pass edge filter (Semrock) to remove the PL signal. The sample was mounted above the objective lens on a piezoelectric scanning stage. Samples were scanned during the course of the measurement over an area of $5 \times 5 \mu\text{m}$ to avoid photodamage.

Supporting Information

Supporting Information is available from the Wiley Online Library or from the author.

Acknowledgements

The authors would like to thank Dr. A. Loiudice and Prof. R. Buonsanti for helpful discussions on the precursor

interactions and ALD processes. This work was performed at the Molecular Foundry, supported by the Office of Science, Office of Basic Energy Sciences, of the U.S. Department of Energy under contract no. DE-AC02-05CH11231. A.W.-B. was supported by the U.S. Department of Energy Early Career Award. M.L. was supported by NSET DOE program. Materials synthesis and characterization was also funded by the U.S. Department of Energy, Office of Science, Office of Basic Energy Sciences, Materials Sciences and Engineering Division, under contract no. DE-AC02-05-CH11231 (inorganic/organic nanostructures program KC3104).

Conflict of Interest

The authors declare no conflict of interest.

Keywords

atomic layer deposition, exciton diffusion, optical properties, passivation, perovskite nanocrystals

Received: June 3, 2020

Revised: July 10, 2020

Published online: July 30, 2020

- [1] M. V. Kovalenko, L. Protesescu, M. I. Bodnarchuk, *Science* **2017**, *358*, 745.
- [2] L. Protesescu, S. Yakunin, M. I. Bodnarchuk, F. Krieg, R. Caputo, C. H. Hendon, R. X. Yang, A. Walsh, M. V. Kovalenko, *Nano Lett.* **2015**, *15*, 3692;
- [3] Y. Li, X. Zhang, H. Huang, S. V. Kershaw, A. L. Rogach, *Mater. Today* **2020**, *32*, 204.
- [4] Q. A. Akkerman, V. D'Innocenzo, S. Accornero, A. Scarpellini, A. Petrozza, M. Prato, L. Manna, *J. Am. Chem. Soc.* **2015**, *137*, 10276.
- [5] a) V. Pinchetti, A. Anand, Q. A. Akkerman, D. Sciacca, M. Lorenzon, F. Meinardi, M. Fanciulli, L. Manna, S. Brovelli, *ACS Energy Lett.* **2019**, *4*, 85; b) P. Todorović, D. Ma, B. Chen, R. Quintero-Bermudez, M. I. Saidaminov, Y. Dong, Z.-H. Lu, E. H. Sargent, *Adv. Opt. Mater.* **2019**, *7*, 1901440.
- [6] a) K. X. Steirer, P. Schulz, G. Teeter, V. Stevanovic, M. Yang, K. Zhu, J. J. Berry, *ACS Energy Lett.* **2016**, *1*, 360; b) M. Pandey, K. W. Jacobsen, K. S. Thygesen, *J. Phys. Chem. Lett.* **2016**, *7*, 4346; c) K. Miyata, D. Meggiolaro, M. T. Trinh, P. P. Joshi, E. Mosconi, S. C. Jones, F. De Angelis, X.-Y. Zhu, *Sci. Adv.* **2017**, *3*, e1701217; d) H. Huang, M. I. Bodnarchuk, S. V. Kershaw, M. V. Kovalenko, A. L. Rogach, *ACS Energy Lett.* **2017**, *2*, 2071; e) J. Kang, L.-W. Wang, *J. Phys. Chem. Lett.* **2017**, *8*, 489; f) D. N. Dirin, L. Protesescu, D. Trummer, I. V. Kochetygov, S. Yakunin, F. Krumeich, N. P. Stadie, M. V. Kovalenko, *Nano Lett.* **2016**, *16*, 5866.
- [7] a) J. Li, L. Xu, T. Wang, J. Song, J. Chen, J. Xue, Y. Dong, B. Cai, Q. Shan, B. Han, *Adv. Mater.* **2017**, *29*, 1603885; b) T. Chiba, K. Hoshi, Y.-J. Pu, Y. Takeda, Y. Hayashi, S. Ohisa, S. Kawata, J. Kido, *ACS Appl. Mater. Interfaces* **2017**, *9*, 18054
- [8] a) S. Yakunin, L. Protesescu, F. Krieg, M. I. Bodnarchuk, G. Nedelcu, M. Humer, G. De Luca, M. Fiebig, W. Heiss, M. V. Kovalenko, *Nat. Commun.* **2015**, *6*, 8056; b) S. W. Eaton, M. Lai, N. A. Gibson, A. B. Wong, L. Dou, J. Ma, L.-W. Wang, S. R. Leone, P. Yang, *Proc. Natl. Acad. Sci. USA* **2016**, *113*, 1993.
- [9] a) A. Swarnkar, A. R. Marshall, E. M. Sanehira, B. D. Chernomordik, D. T. Moore, J. A. Christians, T. Chakrabarti, J. M. Luther, *Science* **2016**, *354*, 92; b) Q. A. Akkerman, M. Gandini, F. Di Stasio, P. Pastogi, F. Palazon, G. Bertoni, J. M. Ball, M. Prato, A. Petrozza, L. Manna, *Nat. Energy* **2017**, *2*, 16194; c) F. Li, S. Zhou, J. Yuan, C. Qin, Y. Yang, J. Shi, X. Ling, Y. Li, W. Ma, *ACS Energy Lett.* **2019**, *4*, 2571
- [10] F. Meinardi, Q. A. Akkerman, F. Bruni, S. Park, M. Mauri, Z. Dang, L. Manna, S. Brovelli, *ACS Energy Lett.* **2017**, *2*, 2368.
- [11] a) B. J. Bohn, Y. Tong, M. Gramlich, M. L. Lai, M. Döblinger, K. Wang, R. L. Z. Hoye, P. Müller-Buschbaum, S. D. Stranks, A. S. Urban, L. Polavarapu, J. Feldmann, *Nano Lett.* **2018**, *18*, 5231; b) M. Lorenzon, L. Sortino, Q. Akkerman, S. Accornero, J. Pedrini, M. Prato, V. Pinchetti, F. Meinardi, L. Manna, S. Brovelli, *Nano Lett.* **2017**, *17*, 3844; c) Y.-S. Park, S. Guo, N. S. Makarov, V. I. Klimov, *ACS Nano* **2015**, *9*, 10386; d) M. J. Jurow, T. Lampe, E. Penzo, J. Kang, M. A. Koc, T. Zechel, Z. Nett, M. Brady, L. W. Wang, A. P. Alivisatos, S. Cabrini, W. Brutting, Y. Liu, *Nano Lett.* **2017**, *17*, 4534; e) S. Bittner, S. Guazzotti, Y. Zeng, X. Hu, H. Yilmaz, K. Kim, S. S. Oh, Q. J. Wang, O. Hess, H. Cao, *Science* **2018**, *361*, 1225.
- [12] N. Kholmicheva, P. Moroz, H. Eckard, G. Jensen, M. Zamkov, *ACS Energy Lett.* **2017**, *2*, 154.
- [13] E. Penzo, A. Loiudice, E. S. Barnard, N. J. Borys, M. J. Jurow, M. Lorenzon, I. Rajzbaum, E. K. Wong, Y. Liu, A. M. Schwartzberg, S. Cabrini, S. Whitlam, R. Buonsanti, A. Weber-Bargioni, *ACS Nano* **2020**, *14*, 6999.
- [14] G. M. Akselrod, F. Prins, L. V. Poulikakos, E. M. Y. Lee, M. C. Weidman, A. J. Mork, A. P. Willard, V. Bulović, W. A. Tisdale, *Nano Lett.* **2014**, *14*, 3556.
- [15] M. Yang, P. Moroz, E. Miller, D. Porotnikov, J. Cassidy, C. Ellison, X. Medvedeva, A. Klinkova, M. Zamkov, *ACS Photonics* **2020**, *7*, 154.
- [16] a) S. N. Raja, Y. Bekenstein, M. A. Koc, S. Fischer, D. Zhang, L. Lin, R. O. Ritchie, P. Yang, A. P. Alivisatos, *ACS Appl. Mater. Interfaces* **2016**, *8*, 35523; b) A. Loiudice, S. Saris, E. Oveisi, D. T. L. Alexander, R. Buonsanti, *Angew. Chem.* **2017**, *56*, 10696; c) S. Saris, S. T. Dona, V. Niemann, A. Loiudice, R. Buonsanti, *Helvetica Chim. Acta* **2020**, *103*, e2000055; d) M. J. Jurow, T. Morgenstern, C. Eisler, J. Kang, E. Penzo, M. Do, M. Engelmayer, W. T. Osowiecki, Y. Bekenstein, C. Tassone, *Nano Lett.* **2019**, *19*, 2489.
- [17] a) G. Li, F. W. R. Rivarola, N. J. L. K. Davis, S. Bai, T. C. Jellicoe, F. de la Peña, S. Hou, C. Ducati, F. Gao, R. H. Friend, N. C. Greenham, Z.-K. Tan, *Adv. Mater.* **2016**, *28*, 3528; b) F. Palazon, Q. A. Akkerman, M. Prato, L. Manna, *ACS Nano* **2016**, *10*, 1224.
- [18] a) H. Huang, B. Chen, Z. Wang, T. F. Hung, A. S. Susha, H. Zhong, A. L. Rogach, *Chem. Sci.* **2016**, *7*, 5699; b) M. Meyns, M. Perálvarez, A. Heuer-Jungemann, W. Hertog, M. Ibáñez, R. Nafria, A. Genç, J. Arbiol, M. V. Kovalenko, J. Carreras, A. Cabot, A. G. Kanaras, *ACS Appl. Mater. Interfaces* **2016**, *8*, 19579; c) H. Huang, H. Lin, S. V. Kershaw, A. S. Susha, W. C. Choy, A. L. Rogach, *J. Phys. Chem. Lett.* **2016**, *7*, 4398.
- [19] a) J. L. van Hemmen, S. B. S. Heil, J. H. Klootwijk, F. Roozeboom, C. J. Hodson, M. C. M. van de Sanden, W. M. M. Kessels, *J. Electrochem. Soc.* **2007**, *154*, G165; b) A. M. Schwartzberg, D. Olynick, *Adv. Mater.* **2015**, *27*, 5778.
- [20] R. L. Puurunen, *J. Appl. Phys.* **2005**, *97*, 121301.
- [21] S. Heil, P. Kudlacek, E. Langereis, R. Engeln, M. A. van de Sanden, W. Kessels, *Appl. Phys. Lett.* **2006**, *89*, 131505.
- [22] a) L. Jethi, M. M. Krause, P. Kambhampati, *J. Phys. Chem. Lett.* **2015**, *6*, 718; b) M. M. Krause, J. Mooney, P. Kambhampati, *ACS Nano* **2013**, *7*, 5922.